CCS Chemistry

RESEARCH ARTICLE

Received: Nov. 30, 2020 | Accepted: Feb. 18, 2021 | Published: Mar. 30, 2021

An Artemisinin Derivative ART1 Induces Ferroptosis by Targeting the HSD17B4 Protein Essential for Lipid Metabolism and Directly Inducing Lipid Peroxidation

Jingjing Xie[1,2†], Guangya Zhu[1,2†], Ming Gao[3†], Jie Xi[3], Ge Chen[4], Xinxin Ma[1], Yu Yan[5], Zhiyuan Wang[1,2], Ze-Jun Xu[6], Hui-Jun Chen[6], Hong-Dong Hao[6], Yaoyang Zhang[1], Zhu-Jun Yao[3*] & Jidong Zhu[1,7*]

[1]Interdisciplinary Research Center on Biology and Chemistry, Shanghai Institute of Organic Chemistry, Chinese Academy of Sciences, Shanghai 201203, [2]University of the Chinese Academy of Sciences, Beijing 100049, [3]State Key Laboratory of Coordination Chemistry, Jiangsu Key Laboratory of Advanced Organic Materials, School of Chemistry and Chemical Engineering, Nanjing University, Nanjing, Jiangsu 210023, [4]School of Life Sciences, Westlake University, Hangzhou 310012, [5]Department of Translational Research in Psychiatry, Max Planck Institute of Psychiatry, Munich 80804, [6]State Key Laboratory of Bioorganic and Natural Products Chemistry, Shanghai Institute of Organic Chemistry, Chinese Academy of Sciences, Shanghai 200032, [7]Center for Excellence in Molecular Synthesis, Shanghai Institute of Organic Chemistry, Chinese Academy of Sciences, Shanghai 200032

**Corresponding authors: zhujd@sioc.ac.cn; yaoz@nju.edu.cn; †Co-first authors.*

Cite this: *CCS Chem.* **2022**, 4, 304–317
DOI: 10.31635/ccschem.021.202000691

Artemisinin and its derivatives, commonly known as antimalarial drugs, have gradually come to be regarded as potential antitumor agents, although their cytotoxic efficacy and mechanisms of action remain to be settled. Herein, we report that an artemisinin analog, ART1, can potently induce ferroptosis in a subset of cancer cell lines. Structure–activity relationship (SAR) analysis reveals that both the endoperoxide moiety and the artemisinin skeleton are required for the antitumor activity of ART1. Aided with ART1-based small-molecule tools, chemical proteomic analysis identified the HSD17B4 protein as a direct target of ART1. HSD17B4 resides in peroxisomes and is an essential enzyme in the catabolism of very-long-chain fatty acids. Our results demonstrate that ART1 initiates ferroptosis through selective oxidation of the fatty acids in peroxisomes by hijacking the HSD17B4 protein without disturbing its enzymatic function, providing a promising mechanism to develop therapeutics for cancer treatment.

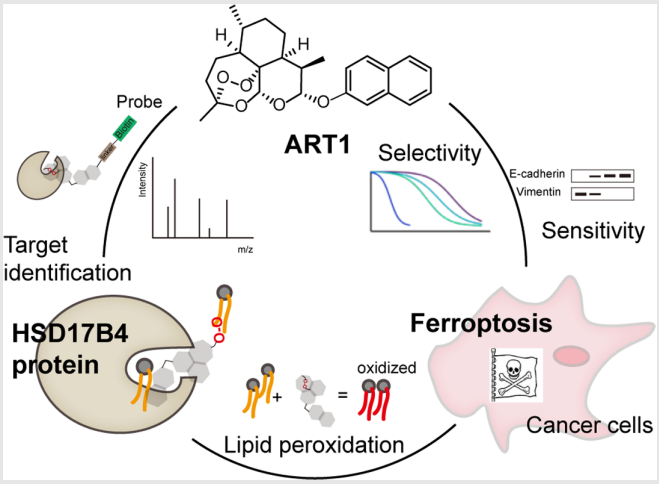

Keywords: artemisinin derivative, antitumor, ferroptosis, HSD17B4, selectivity, mesenchymal

DOI: 10.31635/ccschem.021.202000691
Corrected Citation: *CCS Chem.* **2022**, 4, 304–317
Previous Citation: *CCS Chem.* **2021**, 3, 664–677
Link to VoR: https://doi.org/10.31635/ccschem.021.202000691

Introduction

Cell death is a critical biological process in mammalian development and homeostasis. Some kinds of cell death caused by accidental insults cannot be reversed, but regulated cell death mediated by specific intracellular mechanisms can be modulated with pharmacological and genetic tools. Apoptosis was the first identified form of regulated cell death, but recently other nonapoptotic programmed cell deaths, including necroptosis, pyroptosis, and ferroptosis, have been discovered.[1-3] Ferroptosis is an iron-dependent mode of cell death in which lipid peroxides accumulate to lethal levels.[4-6] Both depletion of reduced glutathione (GSH) levels and inactivation of the lipid-peroxide-reducing enzyme (GPX4) can lead to ferroptotic cell death.[7-10] Meanwhile, oxidative stress and excess iron are associated with cancer progression.[11] Studies have shown that metastasis-prone mesenchymal cancer cells, usually resistant to targeted and chemotherapies are highly sensitive to ferroptosis.[12,13] Consequently, activation of ferroptosis may be a legitimate approach to cancer treatment.[8,10,14-16]

Artemisinin [Qinghaosu (QHS)], a sesquiterpene lactone containing an unusual peroxide bridge, was isolated from the plant *Artemisia annua*, and, together with some of its derivatives, has been recognized as a potent drug for the treatment of malaria.[17,18] It is widely accepted that the iron-mediated cleavage of artemisinin's endoperoxide bridge and further release of highly reactive radicals are responsible for the rapid death of the malaria parasite.[19,20] Recent studies have shown that artemisinins possess antitumor activity in various cancer cell lines derived from leukemia, liver cancer, brain glioma, breast cancer, and colon cancer.[21-25] Although their cytotoxicity against cancer cells is often weak, artemisinins exhibit minimal cytotoxic effects on normal cells and are able to overcome drug resistance.[26,27] The reported cytotoxic effects exerted by artemisinins are complex, including inhibition of cell proliferation, induction of cell apoptosis, arrest of the cell cycle, reduction of angiogenesis, inhibition of cell invasion and metastasis, induction of oxidative damage reactions, and regulation of tumor microenvironment.[23-25,27-30] Previous studies also attempted to identify the protein target(s) of artemisinin and decipher the molecular mechanisms by which artemisinins kill cancer cells, but to date, the exact antitumor-related targets of artemisinins have not been clearly identified.[11,29,31-34] It suggests that artemisinins may target a broad spectrum of protein substrates in mammalian cells, and the specificity of artemisinins treating cancers with mechanism-based patient stratification has become an issue.

HSD17B4 protein, also called multifunctional enzyme type 2 (MFE-2) and D-bifunctional protein (DBP), is found in peroxisomes where it plays a central role in peroxisomal β-oxidation.[35] It interacts with most, if not all, peroxisomal β-oxidation substrates and catalyzes the second and third steps of peroxisomal β-oxidation of fatty acids and fatty acid derivatives.[36,37] It is a 79 kDa homodimeric enzyme, and each monomer has three functional units: a (3*R*)-hydroxyacyl-CoA dehydrogenase unit, a 2-enoyl-CoA hydratase 2 unit, and a sterol carrier protein 2-like (SCP-2L) unit.[38-40] HSD17B4 protein is responsible for the breakdown of very-long-chain fatty acids (VLCFA) such as C26:0, long-chain polyunsaturated fatty acids (PUFA), including C24:6, branched-chain fatty acids, and bile acid intermediates.[35] Although the function of HSD17B4 in the metabolism of fatty acid has been well studied, its role in ferroptosis and its linkage with the anticancer action of artemisinin and its derivatives have not been explored.

In this study, a preliminary screening of our laboratory-made small library of artemisinin derivatives and analogs showed that ART1, an artemisinin derivative bearing a naphthalene unit [(3*R*,5a*S*,6*R*,9*R*,10*R*,12*R*,12a*R*)-3,6,9-trimethyl-10-(naphthalen-2-yloxy)decahydro-12*H*-3,12-epoxy[1,2]-dioxepino-[4,3-i]isochromene, Figure 1a] exhibits potent and selective anti-proliferative activity against cancer cell lines over normal cells. Mechanistic studies indicate that ART1 inhibits cancer cell viability through induction of noncanonical ferroptosis without affecting its intracellular GSH level and GPX4 activity. Further chemical proteomic studies revealed that the HSD17B4 protein, which is involved in the β-oxidation of VLCFA, is the direct target of ART1. Our finding that artemisinin analog ART1 targets HSD17B4 protein in peroxisome may represent a novel selective antitumor mechanism through induction of ferroptotic cell death.

Experimental Methods

Cell lines

Cells were maintained according to the guidance from American Type Culture Collection. Human HEK293T (female) and HEK293FT (female) cells were cultured in Dulbecco's modified Eagle's medium (DMEM) supplemented with 10% (v/v) fetal bovine serum (FBS), 100 units/mL penicillin and 100 mg/mL streptomycin. Human NCI-H1838 (female), NCI-H1975 (female), NCI-H1650 (male), NCI-H1299 (male), A549 (male), and MV4;11 (male) cells were cultured in RPMI1640 supplemented with 10% (v/v) FBS, 100 units/mL penicillin and 100 mg/mL streptomycin. All cells were cultured at 37 °C in a humidified atmosphere of 95% air and 5% CO_2. Cells obtained from the cell bank of Shanghai Institute of Biochemistry and Cell Biology (Shanghai, China) and Cobioer Company (Nanjing, Jiangsu Province, China) were authenticated by short tandem repeat (STR) analysis and mycoplasma detection. Other cells were verified

DOI: 10.31635/ccschem.021.202000691
Corrected Citation: *CCS Chem.* **2022**, 4, 304–317
Previous Citation: *CCS Chem.* **2021**, 3, 664–677
Link to VoR: https://doi.org/10.31635/ccschem.021.202000691

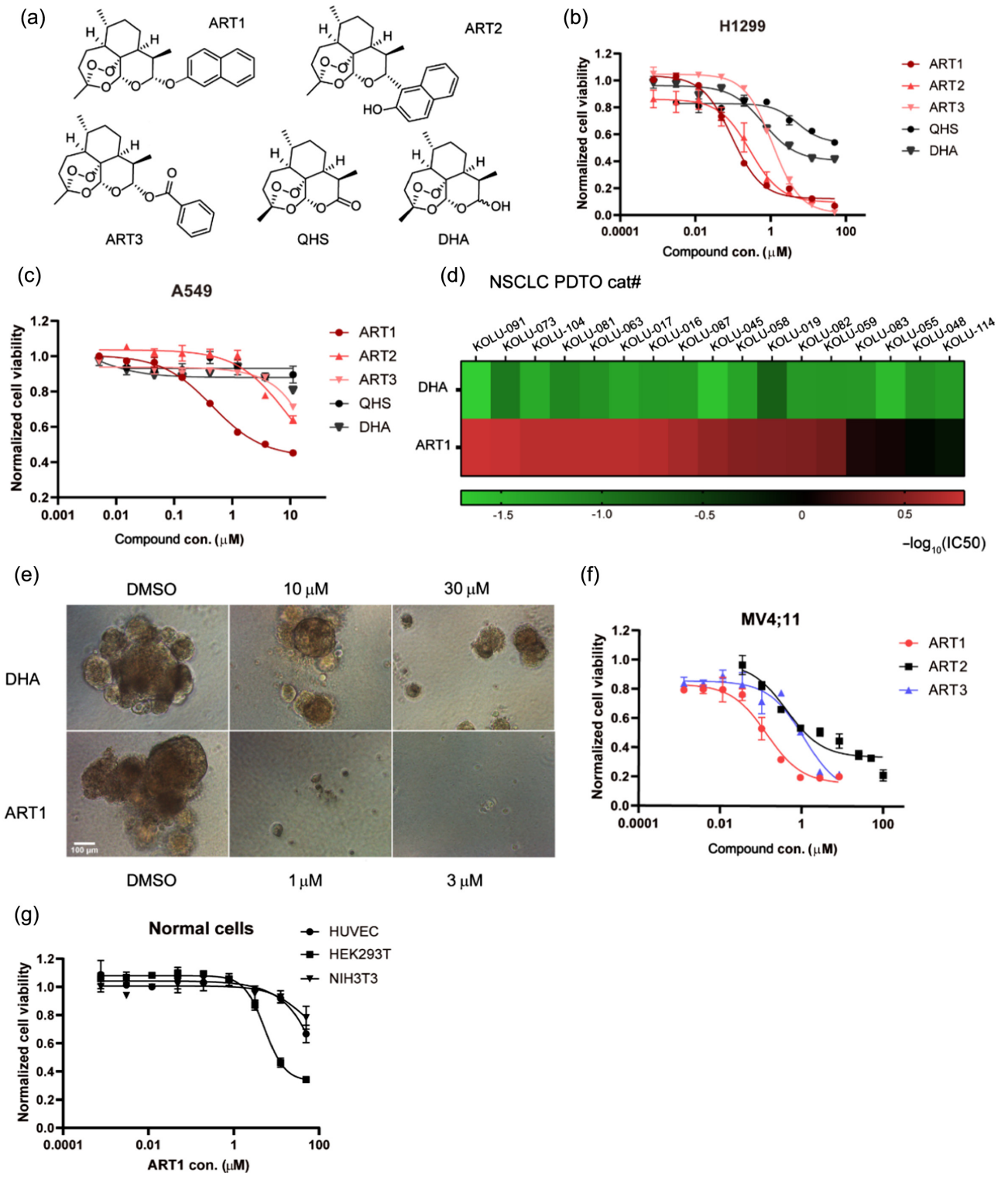

Figure 1 | *ART1 inhibits cancer growth. (a) Structures of ART1, ART2, ART3, and artemisinins (QHS and DHA). (b) Effects of ART1, ART2, ART3, and artemisinins on viability of H1299 cells. Data are represented as mean ± SEM (n = 3). (c) Effects of ART1, ART2, ART3, and artemisinins on viability of A549 cells. Data are represented as mean ± SEM (n = 3). (d) IC50 values of ART1 and DHA against a panel of PDTOs derived from NSCLCs patients. Data are represented as mean ± SEM (n = 2). (e) Representative images showing the anticancer efficacy of ART1 and DHA against PDTOs. Scale bar = 100 μm. (f) Effects of ART1, ART2, and ART3 on the viability of leukemia MV4;11 cells. Data are represented as mean ± SEM (n = 3). (g) Effects of ART1 on the viability of several normal cells. Data are represented as mean ± SEM (n = 3).*

DOI: 10.31635/ccschem.021.202000691
Corrected Citation: *CCS Chem.* **2022**, 4, 304–317
Previous Citation: *CCS Chem.* **2021**, 3, 664–677
Link to VoR: https://doi.org/10.31635/ccschem.021.202000691

through periodic morphology checks and mycoplasma detection.

Patient-derived tumor organoid

Surgery tissues were obtained from patients with advanced non-small cell lung carcinoma (NSCLC) after ethical approval by the Ethics Committee of Hebei People's Hospital (NCT03453307; Shijiazhuang, Hebei, China) and informed consent from all participants or next of kin. The tissues were washed with cold phosphate-buffered saline (PBS) containing antibiotics and chopped into approximately 5 mm pieces with surgical scissors. Tissues were further washed with 10 mL advanced DMEM/F12 (Thermo Fisher Scientific, Waltham, MA) containing 1× Glutamax, 10 mM *N*-(2-hydroxyethyl)piperazine-*N*′-ethanesulfonic acid (HEPES), and antibiotics and digested in 10 mL advanced DMEM/F12 containing 2% fetal calf serum (FCS) and 2 mg/mL collagenase (Sigma, C9407) on an orbital shaker at 37 °C for 1–2 h. The pellet was resuspended in 10 mL advanced DMEM/F12 containing 2% FCS and centrifuged again at 400*g*. Dissociated cells were collected in advanced DMEM/F12 (Thermo Fisher Scientific), suspended in growth factor reduced (GFR) matrigel (Corning Inc., Corning, NY), and seeded. The matrigel was then solidified and overlaid with 500 μL of complete human organoid medium, which was subsequently refreshed every 2 days. Patient-derived tumor organoids (PDTOs) were cultured in advanced DMEM/F12, supplemented with 1× B27 additive and 1× N2 additive (Thermo Fisher Scientific), 0.01% bovine serum albumin (BSA), 2 mM L-glutamine, 100 units/mL penicillin-streptomycin, and containing the following additives: epidermal growth factor (EGF), noggin, R-spondin 1, gastrin, FGF-10 (FGF = fibroblast growth factor), FGF-basic, Wnt-3A, prostaglandin E2, Y-27632, nicotinamide, A83-01, A83-01, SB202190, and hepatocyte growth factor (HGF) (Pepro-Tech, London, UK). Passaging of patient derived organoids (PDOs) was performed using TrypLE (Thermo Fisher Scientific). PDOs were biobanked in FBS (Thermo Fisher Scientific), containing 10% dimethyl sulfoxide (DMSO) (Sigma-Aldrich, St. Louis, MI). Experiments were performed with two biological replicates.

ART16 pull down from cell lysates

H1299 and MV4;11 cells incubated with 10 μM ART16 or biotin for 2 h were harvested and lysed in lysis buffer (50 mM Tris–HCl 7.5, 150 mM NaCl, 0.4% NP40, 1.5 mM $MgCl_2$, 1 mM dithiothreitol (DTT), 5% glycerol, 1% proteinase cocktail). Then transferred supernatants were incubated with 30 μL streptavidin-agarose (20359; Thermo Fisher Scientific) for 40 min at room temperature. The beads were washed four times with lysis buffer. The precipitates were analyzed by silver staining or western blot with anti-HSD17B4 antibody. Experiments were performed three independent times.

ART16 pull down with purified protein

Purified HSD17B4 protein (final, 1 μM) was pretreated with increasing concentrations of ART1 for 1 h followed by treatment with 5 μM ART16 for 2 h and was further incubated with Dynabeads MyOne (65002; Thermo Fisher Scientific) for 1.5 h at 4 °C. The beads were washed with PBST (phosphate buffer saline, 0.05% Tween-20). The precipitates were analyzed by western blotting with anti-HSD17B4 antibody. Experiments were performed three independent times.

Assessment of lipid peroxidation with c11-BODIPY

H1299 cells were seeded in a six-well plate prior to the experiment so that the cell density reached 70–80% confluency at the day of ART1 treatment. Cells were treated with DMSO or 5 μM ART1 with or without deferoxamine (DFO; 100 μM) and incubated for 6 h at 37 °C. Then cells were harvested by trypsinization, washed, and resuspended in PBS containing 1 μM c11-BODIPY (4,4-difluoro-3a,4a-diaza-s-indacene; Thermo Fisher Scientific) and incubated for 30 min at 37 °C. Fluorescence intensity was measured on the FL1 channel with gating to rule out dead cells; 10,000 cells were analyzed per condition. Experiments were performed three independent times.

Intracellular GSH/GSSG measurement

H1299 cells were treated with vehicle (DMSO) or ART1 (10 μM) for 7 and 24 h: one set of cells was used for total GSH measurement, and the other set of cells was used for oxidized glutathione (GSSG) measurement. Treatments were then removed and replaced with corresponding lysis reagent provided in the GSH/GSSG-Glo Assay (Promega V6611). The intracellular GSH/GSSG levels were examined per the kit's assay protocol. Experiments were performed with three biological replicates.

GPX4 activity assay using *tert*-butyl hydroperoxide

H1299 cells with 80% confluency in a 10 cm dish were treated with vehicle (DMSO), ART1(10 μM) for 12 h, or RSL3 (1 μM) for 2 h. Cells were harvested by trypsinization, washed twice in PBS, and resuspended in lysis buffer (25 mM Tris–HCl, pH 8.0, 150 mM NaCl, 0.3% Triton X-100, 0.1 mM DFO). Cells were further sonicated on ice for 20 min and centrifuged at 14,000*g* for 15 min. The Bradford method was used to measure the protein concentration in cell lysates. Enzymatic reactions were performed in 96-well microplate (100 μL volume). In lysis buffer containing reduced nicotinamide adenine

DOI: 10.31635/ccschem.021.202000691
Corrected Citation: *CCS Chem.* **2022**, 4, 304–317
Previous Citation: *CCS Chem.* **2021**, 3, 664–677
Link to VoR: https://doi.org/10.31635/ccschem.021.202000691

dinucleotide phosphate (NADPH) (final 0.25 mM), GSH reductase (final 0.5 U/mL, Sigma G3664), 1.40 μg/μL cell lysates were added and mixed. The enzymatic reaction was initiated by adding 1 μL of 30 mM *tert*-butyl hydroperoxide (*t*-BuOOH) (Sigma 458139) to the reaction mixture. The depletion of NADPH was examined kinetically by reading OD340 at 10 s intervals over 30 min. Experiments were performed with two biological replicates.

Biolayer interferometry

The binding between ART16 and HSD17B4 protein was examined using biolayer interferometry (BLI) Octet RED96 (ForteBio Inc., Menlo Park, CA). Streptavidin biosensors (ForteBio Inc.) were presoaked for 30 min in assay buffer (25 mM Tris–HCl pH 8.0, 150 mM NaCl, 2 mM DTT, 1% BSA, and 0.02% Tween-20), then coated in an assay buffer containing 5 μM ART-16 for 5 min. Sensors were quenched in assay buffer containing 50 μM biocytin for 1 min, followed by a 2 min wash with assay buffer. Indicated concentrations of HSD17B4 protein (4.50, 1.93, 0.82, 0.35, 0.15, and 0.06 μM) were diluted in assay buffer and flowed through biosensors coated with ART16 or biocytin for 5 min. A 10 min dissociation followed. Data were analyzed using OctetRED analysis software. Experiments were performed two independent times.

HSD17B4 protein enzymatic assay

The enzymatic activity of HSD17B4 protein was examined accordingly to the literature procedure.[36] D-3-Hydroxyacyl CoA dehydrogenase assay consists of the following: the 5× assay buffer contains 125 mM Tris–HCl, pH 8.0; 5 mM NAD+; 250 mM KCl; 0.05% Triton X-100, and 0.25% BSA. Purified HSD17B4 protein (1.25 ng/μL) was diluted in assay buffer, coincubated with indicated concentrations of ART1 for 30 min, then 125 μM substrate DL-β-hydroxybutyryl-CoA lithium salt (Sigma H0261) was added, and immediately, the excitation and emission at 340 and 460, respectively, for NADH was measured with a kinetic process to quantify the dehydrogenase reaction. The hydratase assay consists of the following: the 2× assay buffer contains 0.64 M Tris–HCl, pH 7.4; 11.8 mM ethylenediaminetetraacetic acid (EDTA), and 0.012% BSA. Purified HSD17B4 protein (2.50 ng/μL) was diluted in assay buffer, coincubated with indicated concentrations of ART1 for 30 min, then 1 mM substrate Crotonyl CoA (Sigma 28007) was added, and immediately OD280 was measured for the remaining substrate with a kinetic process to quantify the dehydrogenase reaction. Experiments were performed with two biological replicates.

Measurement of lipid peroxidation in vitro

Lipid peroxides were examined per the modified absorbance of products from the reaction with thiobarbituric acid (TBARS).[14,41] Thiobarbituric acid (TBA) solution 0.67% (w/v) was prepared in 10% trichloroacetic acid (TCA) with heating to 65 °C to dissolve the TBA solid. Arachidonic acid (AA; 500 μM) was mixed with 25 μM ART1 without 5 μM $FeSO_4$ at 37 °C for 30 min in buffer containing H_2O with 0.02% Triton-X100. Equal volumes of 0.67% (w/v) TBA in 10% TCA were added to the reaction mixture and vortexed and incubated at 95 °C for 15 min. The MDA-TBA pink adduct formed by the reaction of malondialdehyde (MDA) and TBA was measured colorimetrically at 532 nm. Experiments were performed with three biological replicates.

Chemical synthesis

Unless otherwise noted, all reactions were carried out under a nitrogen atmosphere with dry solvents under anhydrous conditions. Tetrahydrofuran (THF) was distilled immediately from sodium benzophenone ketyl prior to use. Methylene chloride (CH_2Cl_2) was distilled immediately before use from calcium hydride. External bath temperatures were used to record all reaction temperatures. All other solvents were processed per the reference Purification of Laboratory Chemicals (Seventh Edition) (detailed information could be found in Supporting Information Pages S5–S14). Silica gel (300–400 mesh) and petroleum ether, ethyl acetate and acetone were used for product purification by flash column chromatography. Analytical thin-layer chromatography (TLC) was performed with glass TLC plates. Visualization was accomplished with UV light, phosphomolybdic acid staining, and subsequent heating. ^{1}H and ^{13}C NMR spectra were recorded on either 400 or 500 MHz instruments (Bruker AM-400 spectrometer). IR spectra were recorded on a Fourier Transform infrared spectrometer and listed in cm^{-1}. High-resolution mass spectrometry (HRMS) analyses were determined on a Agilent 6540 quadrupole time-of-flight mass spectrometer(Q-TOF MS). Optical rotations were measured with a polarimeter with a sodium lamp. Detailed synthesis processes are listed in the Supporting Information.

Results and Discussion

Cytotoxicity screen identifies ART1 as a potential antitumor agent

To identify the lead compound derived from artemisinin (QHS) for cancer treatment, a series of endoperoxide derivatives that maintain the artemisinin scaffold but with different aryl substituents in the C-10 position (ART1, ART2, and ART3) were prepared and screened (Figure 1a, see Supporting Information for detailed information). We compared the antitumor activities of these compounds together with artemisinin (QHS) and its derivative dihydroartemisinin (DHA) in two lung cancer cell lines: H1299

DOI: 10.31635/ccschem.021.202000691
Corrected Citation: *CCS Chem.* **2022**, 4, 304–317
Previous Citation: *CCS Chem.* **2021**, 3, 664–677
Link to VoR: https://doi.org/10.31635/ccschem.021.202000691

Table 1 | *IC50 Values of ART1, ART2 and ART3 against H1299, A549, and MV4;11 Cancer Cells*[a]

Cancer Cells	ART1 (IC50, μM)	ART2 (IC50, μM)	ART3 (IC50, μM)
H1299	0.09 ± 0.01	0.30 ± 0.14	1.19 ± 0.13
A549	0.44 ± 0.03	18.17 ± 6.30	29.10 ± 5.02
MV4;11	0.11 ± 0.01	1.11 ± 0.09	0.45 ± 0.20

[a] Data are represented as mean ± SD (n = 3).

and A549. We found that consistent with previous studies,[11,26,42] QHS and DHA exhibit weak cytotoxic activity in the lung cancer cells with IC50 values ranging from 1 μM to more than 100 μM (Figures 1b and 1c). Among these derivatives, ART1, in which a naphthalene ring attaches to the artemisinin skeleton, exhibited the most potent cytotoxicity against the lung cancer cells (Figures 1b and 1c and Table 1). To determine whether ART1 could inhibit primary cancer cells, we further examined its anti-proliferative efficacy in PDTOs models. Experiments showed that ART1 can suppress the growth of PDTOs derived from NSCLC patients >10-fold more effectively than DHA (Figures 1d and 1e). We further compared the cytotoxicity of ART1, ART2, and ART3 in leukemia MV4;11 cell lines. Again, ART1 was proven to be the most potent compound to inhibit the proliferation of leukemia cells (Figure 1f and Table 1). Modification of the artemisinin skeleton resulted in varied antitumor activity suggesting that, apart from the endoperoxide bridge motif, the artemisinin scaffold also plays a critical role mediating the cancer-cell killing. To prove this, we further screened a library of organic peroxides to compare their antitumor activities (Supporting Information Figure S1).[43,44] Interestingly, although all the compounds contained the peroxide bridge motif, they barely affected the cell proliferation of MV4;11 cells, while ART1 strongly inhibited the cell proliferation. This strongly suggested that the artemisinin skeleton is indispensable for the cytotoxicity of ART1. More importantly, ART1 displays great selectivity, exhibiting very weak anti-proliferative activity against normal cells (Figure 1g). All the above results indicate that ART1 is a promising potential lead of therapeutics for cancer treatment.

ART1 induces noncanonical ferroptotic cell death

Previous reports demonstrate that artemisinins cause death of cancer cells through multiple mechanisms, including apoptosis, autophagy, cell cycle arrest, and inhibition of tumor angiogenesis.[23–25,27–30] We first examined whether apoptosis is induced by ART1 and found that ART1 fails to activate caspases and cause PARP cleavage (Supporting Information Figures S2a and S2b), suggesting that cell death triggered by ART1 is independent of caspase activation and apoptosis. Immunoblotting results indicated that there was no LC3B accumulation upon ART1 treatment, suggesting that autophagy was not mediated in ART1-induced cell death either (Supporting Information Figure S2b). To define the mechanism by which ART1 induces cancer cell death, MV4;11 cells were treated with ART1 at various concentrations alone or with a panel of cell death-suppressing compounds (Figure 2a). The lethality induced by ART1 treatment was only suppressed by the ferroptosis inhibitor ferrostatin-1 which prevents the accumulation of lipid peroxides. It was not suppressed by the apoptosis inhibitor z-VAD-FMK or the necroptosis inhibitor necrostatin-1 (Nec-1).[1] This result clearly showed that ART1 treatment triggers ferroptotic cell death in cancer cells. This conclusion is further supported by the observation that the ART1-induced cell death was rescued in the presence of α-tocopherol, a lipid-soluble anti-oxidant that blocks ferroptosis[4,8,45] in H1299 cells (Figure 2b). We then examined whether ART1 can cause lipid peroxidation, the definitive event of ferroptosis.[6] As shown in Figure 2c, the fluorescence of the lipid peroxidation probe C11-BODIPY monitored by flow cytometry was elevated in H1299 cells treated with ART1, suggesting that the lipid peroxidation was induced by ART1. This elevation was diminished by cotreatment with the iron chelator DFO, confirming that the lipid peroxidation caused by ART1 is iron-dependent. These results indicate that the structural optimization based on artemisinin generated a highly potent compound ART1 that induces cancer cell death through ferroptosis.

We next examined the mechanisms by which ART1 causes ferroptotic cell death and attempted to learn if ART1 behaves like the two canonical classes of ferroptosis inducers, one by decreasing the intracellular levels of GSH, a key cofactor for the lipid-peroxide-reducing enzyme GPX4, and the other by inhibiting GPX4 activity.[4,5,8,10] We quantified the GSH in ferroptosis cells induced by ART1 using a luminescent GSH probe and found that ART1 failed to significantly alter intracellular GSH homeostasis (Figure 2d). This result is consistent with our observation that addition of GSH did not rescue the cell death induced by ART1 treatment (Figure 2a). GPX4 catalyzes the reduction of lipid peroxide to lipid alcohols, making it an important regulator in ferroptotic cell death. The GPX4 activity in H1299 cells was examined using *t*-BuOOH as a surrogate substrate and measuring the rate of NADPH oxidation coupled to the *t*-BuOOH-reducing activity of GPX4.[5,8] We observed an obvious inhibition of GPX4 activity following the treatment with the GPX4 inhibitor RSL3, but the GPX4 activity in ART1-treated cells was comparable with that in control cells (Figure 2e). Moreover, ART1 did not alter the protein levels of GPX4 (Figure 2f). Considering its endoperoxide-containing similarity with another known

DOI: 10.31635/ccschem.021.202000691
Corrected Citation: *CCS Chem.* **2022**, 4, 304–317
Previous Citation: *CCS Chem.* **2021**, 3, 664–677
Link to VoR: https://doi.org/10.31635/ccschem.021.202000691

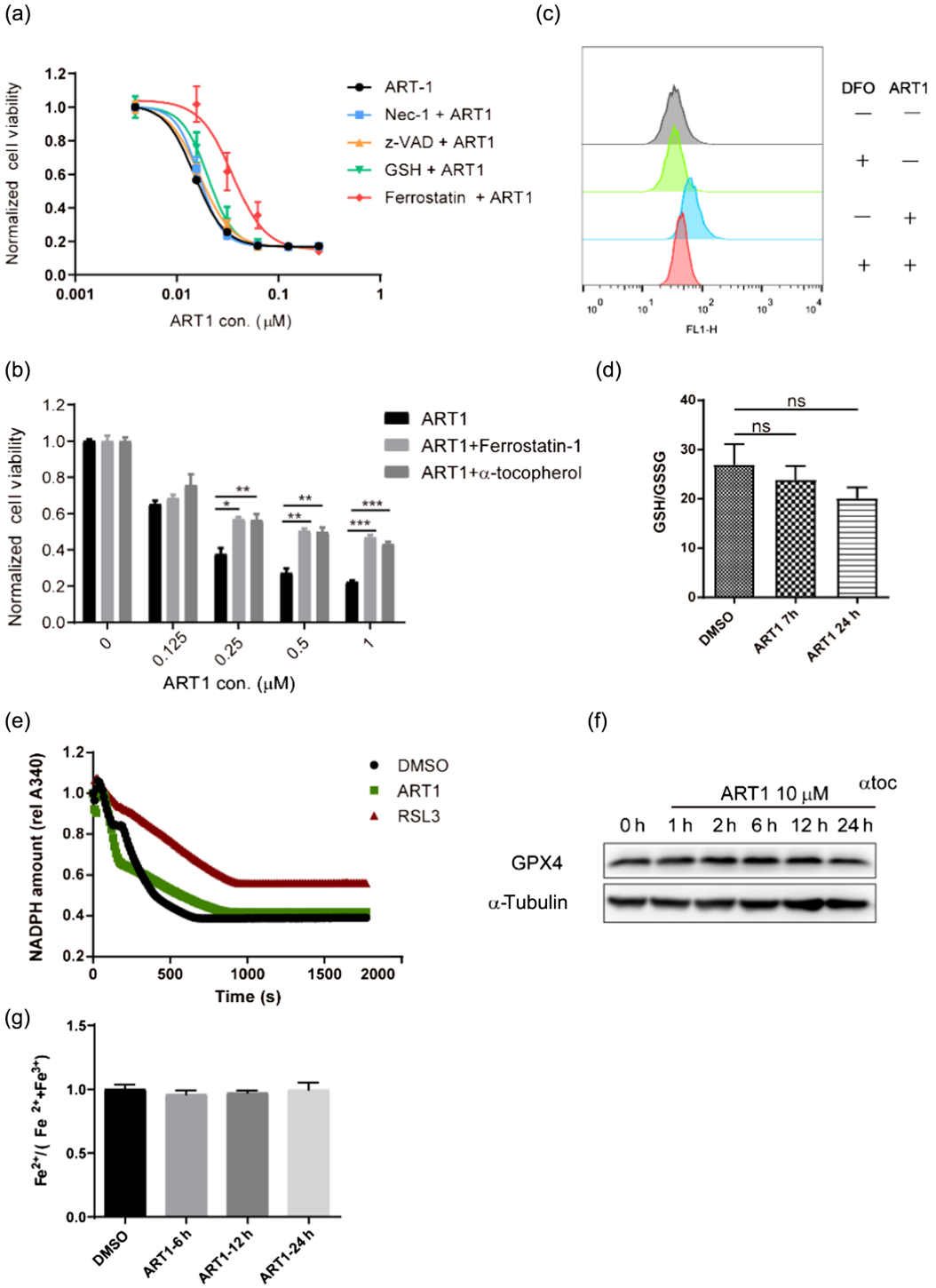

Figure 2 | *ART1 induces cancer cell death through ferroptosis. (a) Effects of various cell death-suppressing compounds on the viability of MV4;11 cells treated with ART1. Data are represented as mean ± SEM (n = 3). (b) Effects of ferroptosis inhibitors on viability of H1299 cells treated with ART1. Data are represented as mean ± SEM (n = 3). *p < 0.05, **p < 0.01, ***p < 0.001. (c) Ability of iron chelator DFO to prevent the production of lipid peroxidation induced by ART1. The experiment was examined by C11-BODIPY using flow cytometry. (d) GSH/GSSG levels in H1299 cells treated with 10 μM ART1. Data are represented as mean ± SEM (n = 3). (e) Effects of the ferroptosis inducers RSL3 and ART1 on GPX4 activity within GPX4-containing cell lysates. The GPX4 activity in H1299 cells was examined using t-BuOOH as a surrogate substrate by measuring the rate of NADPH oxidation coupled to t-BuOOH-reducing activity of GPX4. (f) Immunoblotting result of GPX4 protein in H1299 cells cotreated with ART1 and α-tocopherol. (g) The content of ferrous iron in H1299 cells treated with 5 μM ART1 at indicated time points. Data are represented as mean ± SD (n = 3).*

DOI: 10.31635/ccschem.021.202000691
Corrected Citation: *CCS Chem.* **2022**, 4, 304–317
Previous Citation: *CCS Chem.* **2021**, 3, 664–677
Link to VoR: https://doi.org/10.31635/ccschem.021.202000691

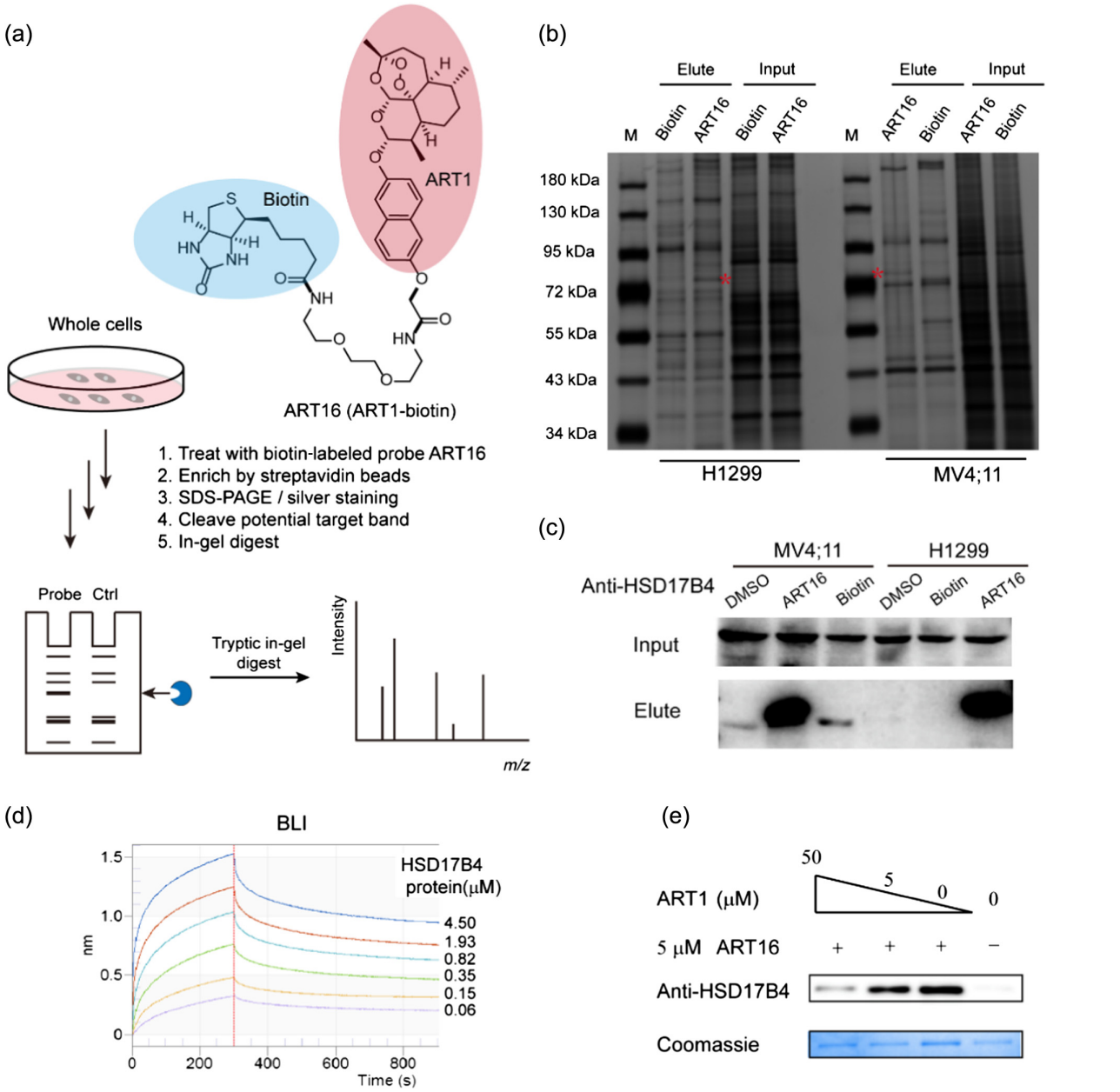

Figure 3 | *ART1 selectively binds to HSD17B4 protein. (a) Structure of biotin-containing ART16 (ART1-biotin) and schematic representation of the biotin-streptavidin pull-down experiments coupled with liquid chromatography mass spectrometry (LC-MS) for the identification of ART1 target protein. (b) Silver staining result of biotin-streptavidin pull-down experiments in MV4;11 and H1299 cells treated with 10 μM ART16 or biotin. The red asterisks indicate the potential binding protein. (c) Immunoblot result of biotin-streptavidin pull-down experiments examined by anti-HSD17B4 protein in MV4;11 and H1299 cells treated with 10 μM ART16 or biotin/DMSO. (d) BLI was used to assess the binding kinetics between ART16 and purified HSD17B4 protein. ART16 was immobilized on the streptavidin biosensors and dipped into wells containing increasing concentrations of HSD17B4 protein. (e) Competitive profiling of the reactivity of ART16 with ART1. Purified HSD17B4 proteins were pretreated with increasing concentrations of ART1 followed by treatment with 5 μM ART16 and then subjected to biotin-streptavidin affinity purification.*

ferroptosis inducer FINO2,[8] we investigated whether ART1 oxidized ferrous iron just like FINO2. However, the content of ferrous iron was not affected by the ART1 treatment (Figure 2g). Taken together, ART1 does not behave like known classes of ferroptosis inducers.

Identification of HSD17B4 protein as a direct target of ART1

To identify the protein target of ART1 mediating the induced ferroptosis, we designed and synthesized a

DOI: 10.31635/ccschem.021.202000691
Corrected Citation: *CCS Chem.* **2022**, 4, 304–317
Previous Citation: *CCS Chem.* **2021**, 3, 664–677
Link to VoR: https://doi.org/10.31635/ccschem.021.202000691

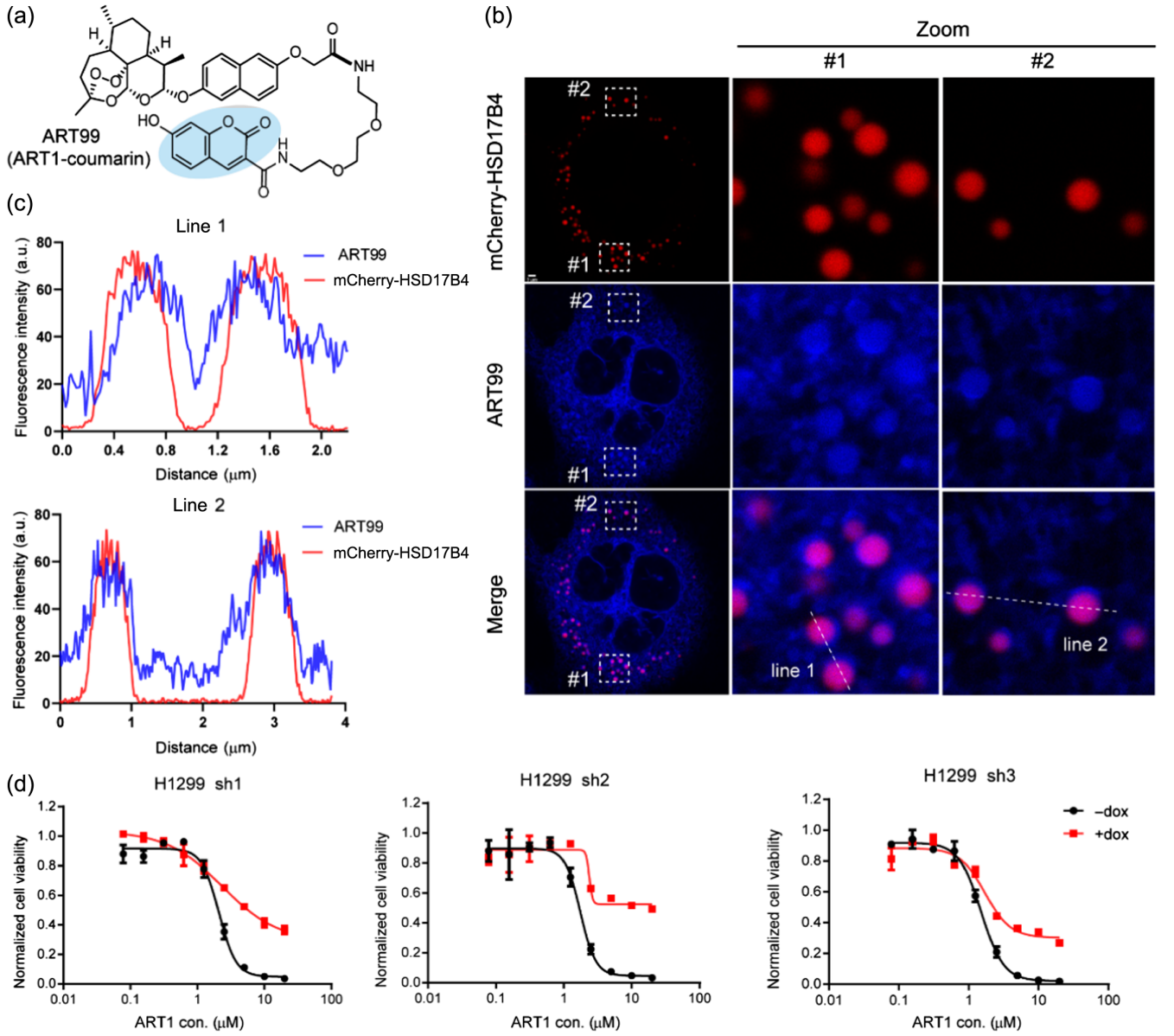

Figure 4 | *ART1 induces cancer cell death through HSD17B4 protein. (a) Structure of ART99 with coumarin fluorophore. (b) Microscopic image of the colocalization analysis with HSD17B4 protein in cells. MEF cells stably expressing mCherry-HSD17B4 were treated with ART99 (ART1-coumarin) for 30 min. Scale bar, 3 μm. (c) Quantification of fluorescence intensity of ART99 and mCherry-HSD17B4 protein along lines 1 and 2 indicated in merged image of (b). (d) Effects of shRNAs targeting HSD17B4 protein on the antitumor efficacy of ART1. Data are represented as mean ± SEM (n = 3).*

biotin-tagged tool compound ART16 (see Supporting Information for detailed information). ART16 retained the potent antitumor activity by inducing ferroptosis similar to ART1 (Supporting Information Figure S3) and was used for subsequent experiments (Figure 3a). H1299 and MV4;11 cells were incubated for 3 h with ART16 or biotin as a negative control and followed by affinity pulldown. Proteins enriched by streptavidin beads were subjected to silver staining and the result revealed a clear band at 79 kDa in the ART16-treated samples but not in the biotin-treated samples from both H1299 and MV4;11 cells (Figure 3b). The potential target band was isolated by retrieving the 79 kDa band from the gel and was subjected to mass spectrometric analysis. Proteomic analysis revealed that peroxisomal MFE-2, the HSD17B4 protein, was highly enriched in the 79 kDa band. Immunoblotting studies confirmed that endogenous HSD17B4 protein can be pulled down from cell lysates by streptavidin agarose in the presence of ART16 (Figure 3c).

DOI: 10.31635/ccschem.021.202000691
Corrected Citation: *CCS Chem.* **2022**, 4, 304–317
Previous Citation: *CCS Chem.* **2021**, 3, 664–677
Link to VoR: https://doi.org/10.31635/ccschem.021.202000691

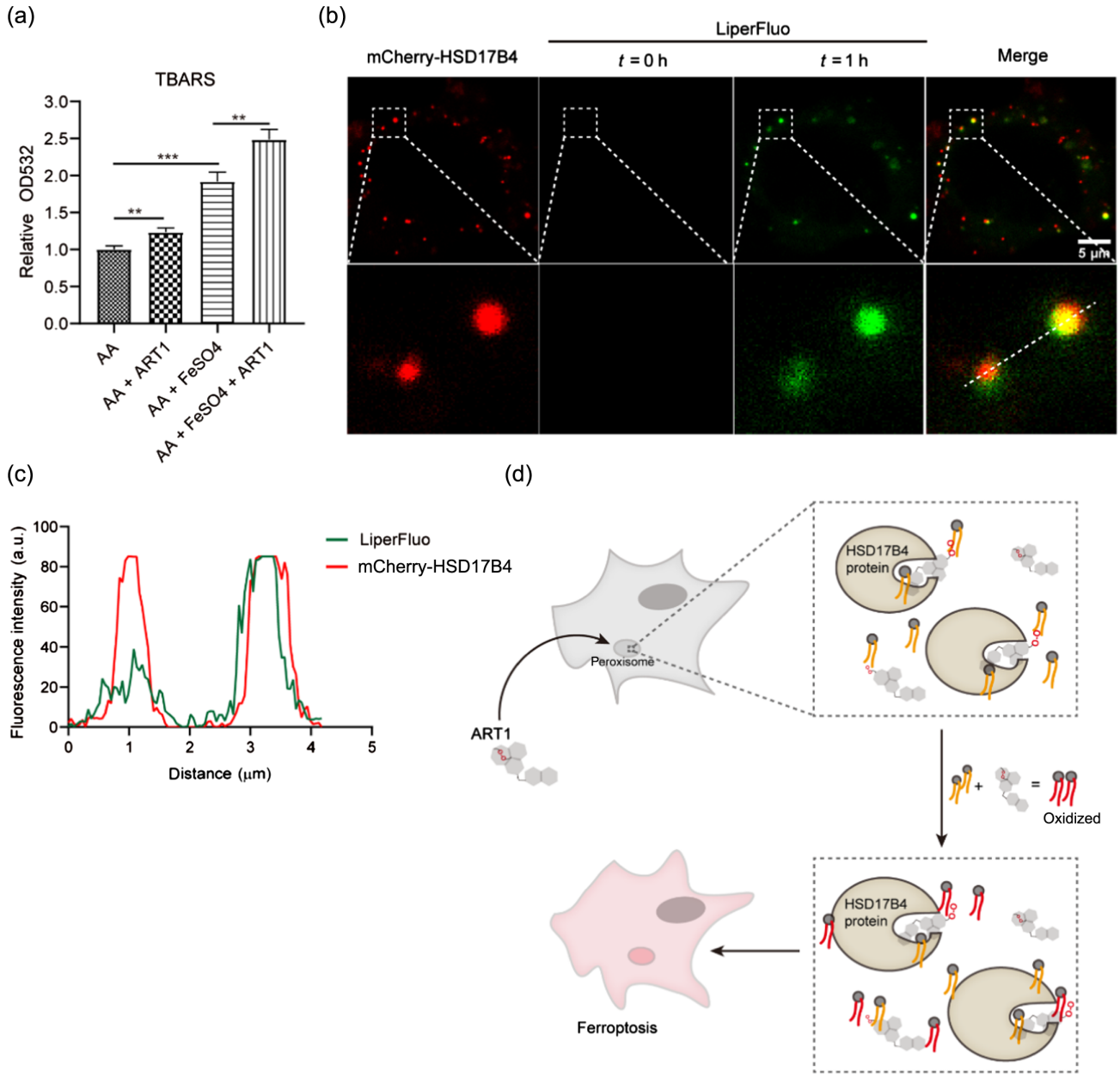

Figure 5 | *ART1 directly oxidizes lipids surrounding the HSD17B4 protein. (a) Ability of ART1 to increase accumulation in vitro of TBARS. Data are represented as mean ± SEM* (n = 3). **p < 0.01, ***p < 0.001. *(b) Live cell fluorescence imaging of lipid peroxides in mCherry–HSD17B4 protein expressing MEF cells treated with ART1. Scale bar, 5 μm. (c) Quantification of fluorescence intensity of LiperFluo and mCherry–HSD17B4 protein along the white line in merged image of (b). (d) ART1 binds to target HSD17B4 protein and oxidizes lipids surrounding HSD17B4 to induce ferroptotic cell death.*

To determine if ART16 can directly bind to HSD17B4 protein in vitro, we conducted a BLI experiment, an established method for studying biomolecular interactions, to further understand the binding of ART16 to HSD17B4. The biotin-labeled compound, ART16, was immobilized on the streptavidin biosensors and dipped into wells containing increasing concentrations of the purified HSD17B4 protein. A clear dose-dependent binding was observed but also a slow dissociation, which indicated a long residence time of the ligand and tight binding between ART16 and HSD17B4 protein (Figure 3d). Pretreatment of HSD17B4 protein with increasing concentrations of ART1, followed by ART16 in a biotin-streptavidin pulldown assay, led to a dose-dependent competition (Figure 3e) indicating that HSD17B4 protein is the direct target of ART1.

DOI: 10.31635/ccschem.021.202000691
Corrected Citation: *CCS Chem.* **2022**, 4, 304–317
Previous Citation: *CCS Chem.* **2021**, 3, 664–677
Link to VoR: https://doi.org/10.31635/ccschem.021.202000691

ART1 triggers cancer cell death mediated by HSD17B4 protein

To visualize the cellular localization of the ART1 binding target, we employed an ART1 probe, ART99 containing a coumarin fluorophore (Figures 4a and Supporting Information Figure S4a). Microscopic images revealed a cytoplasmic distribution of ART99 and colocalization with mCherry-labelled HSD17B4 protein [Mander's correlation coefficient (MCC) = 0.769 for region 1, MCC = 0.841 for region 2; Figures 4b and 4c], while the coumarin control failed to do so (Supporting Information Figure S4b). We then inquired whether the cell death induced by ART1 is mediated by HSD17B4. We examined the antitumor activity of ART1 in H1299 cells stably expressing doxycycline-inducible shRNA targeting HSD17B4 without doxycycline. Three distinct shRNAs were employed and the knockdown efficiency of HSD17B4 was confirmed by immunoblotting (Supporting Information Figure S4c). The HSD17B4 knockdown was found to attenuate significantly the cytotoxicity of ART1 (Figure 4d). To evaluate the specificity of HSD17B4 in sensitization of ART1, HSD17B4 knockdown H1299 cells were treated with several inhibitors of the mitochondrial electron transport chain and kinases. HSD17B4 knockdown cells failed to show multidrug resistance properties but were highly resistant to ART1 (Supporting Information Figure S4d). These data suggest that ART1 exerts its antitumor activity specifically on the target protein, HSD17B4.

ART1 induces direct lipid oxidation through target HSD17B4 protein

HSD17B4 protein is a bifunctional enzyme that possesses both dehydrogenase and hydratase activity, and is involved in the peroxisomal β-oxidation of VLCFA (Supporting Information Figure S5a).[35,36,39,40] We found that incubation of the HSD17B4 protein with ART1 did not alter the abundance of HSD17B4 protein in cells (Supporting Information Figure S5b). Interestingly, neither the dehydrogenase nor the hydratase activity was affected by ART1 (Supporting Information Figures S5c and S5d). Since the peroxide moiety in ART1 is indispensable for induction of ferroptosis, we hypothesized that ART1 might be a selective oxidant that initiates ferroptosis after binding to HSD17B4 and facilitating the oxidation of surrounding lipids. To test this hypothesis, we examined if ART1 could directly oxidize substrates relevant to ferroptosis. PUFA, which are susceptible to lipid peroxidation because they contain bis-allylic hydrogen atoms that can be easily abstracted, are necessary for the execution of ferroptosis.[4,6,7,9,46] Since the very-long-chain PUFA is not readily available to us, AA was used as a surrogate substrate. The in vitro lipid peroxidation experiment was carried out by monitoring MDA, the final product of lipid peroxides, using colorimetric detection.[14,41] As shown in Figure 5a, ART1 alone can oxidize AA. ART1 can also significantly facilitate lipid peroxidation catalyzed by ferrous ions. To examine if ART1 could oxidize the lipids surrounding the HSD17B4 protein in cells, we employed live cell imaging with a lipid peroxides probe, LiperFluo. Mouse embryonic fibroblasts (MEF) cells were stably transfected with mCherry-labeled HSD17B4 protein plasmid. As shown in Figures 5b and 5c, ART1 activated lipid peroxides colocalized with mCherry-HSD17B4 (MCC = 0.803 for inset). These data corroborate our hypothesis that ART1 directly oxidizes the lipids proximal to HSD17B4 protein, which is essential in lipid catabolism, accumulating lipid peroxides, and ultimately ferroptosis in cancer cells (Figure 5d).

ART1 preferentially induces ferroptosis in high-mesenchymal state cancer cells

To further investigate the biomarkers of ART1 sensitivity, we examined its effects on the viability of a panel of lung

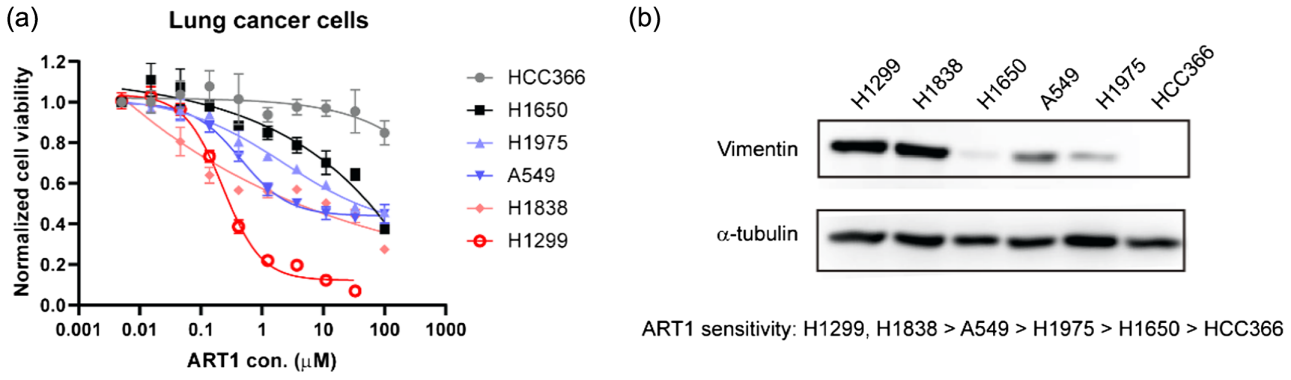

Figure 6 | *The sensitivity of ART1 correlates with the epithelial-mesenchymal state of cancer cells. (a) Antitumor efficacy of ART1 against a panel of lung cancer cells. Data are represented as mean ± SEM (n = 3). (b) Immunoblot result of E-cadherin and vimentin protein level in a panel of lung cancer cell lines.*

DOI: 10.31635/ccschem.021.202000691
Corrected Citation: *CCS Chem.* **2022**, 4, 304–317
Previous Citation: *CCS Chem.* **2021**, 3, 664–677
Link to VoR: https://doi.org/10.31635/ccschem.021.202000691

cancer cells. The sensitivity of these lung cancer cells toward ART1 varies, among which H1299 and H1838 are the most susceptible ones, while H1650 and HCC366 exhibit resistance to ART1 (Figure 6a). It has been reported that therapy-resistant cancer cells in the high-mesenchymal state are susceptible to ferroptosis inducers.[12,13] We examined the epithelial-mesenchymal state of these lung cancer cells by measuring the protein levels of vimentin, a marker of the mesenchymal state. The protein levels of vimentin in sensitive cell lines H1299 and H1838 were considerable, indicating the high-mesenchymal state, whereas resistant HCC366 and H1650 cells exhibit almost undetectable abundance of E-cadherin proteins (Figure 6b). This suggests that the sensitivity of ART1 is well correlated with the epithelial-mesenchymal state of cancer cells, and ART1 could preferentially induce ferroptotic cell death in mesenchymal cancer cells.

Conclusion

In our work, artemisinin derivative ART1 has been identified as a ferroptosis inducer with significant potency and selectivity against cancer cell proliferation. The screenings and IC50 data comparison of the laboratory-made organic peroxides showed that both the peroxide bridge and artemisinin-like hydrocarbon scaffold are necessary for this bioactivity. With structural optimization, ART1 obtains much improved cellular activity with nanomolar-range IC50. More importantly, ART1 shows good selectivity over normal cells. This could be due to the excess oxidative stress and iron abundance associated with cancer progression that endow cancer cell vulnerability to ferroptosis.[11,47,48] Although sporadic research studies indicated that DHA can induce or sensitize cancer cells to ferroptosis through degradation of ferritin,[14,42] the multiple mechanisms and compromised efficacy dampened its usage for cancer treatment. Gaschler et al.[8] have reported that endoperoxide-containing FINO2 triggers ferroptosis through GPX4 inactivation and iron oxidation, suggesting the potential of endoperoxides as ferroptosis-inducing compounds. Here, our findings revealed that the artemisinin-like ART1 boosts cancer cell death through a novel and distinct mechanism without affecting GPX4 activity, GSH state, or iron homeostasis. Moreover, the structurally distinctive ART1 exhibits substantially improved potency over artemisinins and FINO2.

Chemical proteomic approaches aided by ART1-based small-molecule tools led to final identification of HSD17B4 protein, an enzyme essential in the catabolism of VLCFA, as a direct and specific target of ART1. HSD17B4 targeting by ART1 seems to be a conserved mechanism in the ART1-sensitive cancer cells because the ART16 pull-down experiments in both MV4;11 and H1299 cells clearly identified HSD17B4 as the most abundant binding protein. In contrast with previously reported promiscuous binding of multiple proteins by artemisinins,[11,31,34,49] the naphthalene ring appears to endow the artemisinin-like endoperoxide ART1 with some specificity to bind a certain target protein. The HSD17B4 knockdown can attenuate significantly the cytotoxicity of ART1. This work unambiguously links the anticancer action of an artemisinin derivative with ferroptosis via HSD17B4 protein for the first time. Intriguingly, knockdown of HSD17B4 had no effect on cell death triggered by mitochondria or kinase inhibitors, suggesting that HSD17B4 is specifically involved in ferroptosis mediated by ART1. The partial rescue effects of HSD17B4 knockdown and ferroptosis suppressors suggests that ART1 may inhibit cell proliferation through other mechanisms and HSD17B4 protein is one of the targets of ART1.

The significance of the HSD17B4 protein for normal mammalian development and homeostasis is supported by the existence of human diseases such as Perrault syndrome and Zellweger syndrome[35–37] caused by HSD17B4 dysfunction. Notably, our work showed that ART1 causes ferroptosis by directly oxidizing fatty acids surrounding the HSD17B4 protein without disturbing the protein's normal enzymatic activity, revealing an unexpected mechanism where ART1 used HSD17B4 as a "Trojan horse" to sneak into peroxisomes to trigger lipid oxidation. This represents a safe, marginally toxic antitumor therapy and offers new insights into the initiation of ferroptosis.

Many metastasis-prone mesenchymal cancer cells that are insensitive to chemotherapy are vulnerable to ferroptosis inducers.[12,13] ART1 shows great efficacy with mesenchymal cancer cells such as H1299 and H1838 lung cancer cells, highlighting its potential to induce ferroptosis thus coping with drug-resistance and cancer metastasis.

In summary, we report that ART1 potently and selectively induces ferroptosis in a subset of cancer cell lines. Both the endoperoxide moiety and the artemisinin hydrocarbon skeleton are required for the antitumor activity of ART1. Chemical proteomic experiments finally identified HSD17B4 protein, which resides in peroxisomes and is an essential enzyme in the catabolism of VLCFA, as a direct target of ART1. ART1 initiates ferroptosis through selective oxidation of the fatty acids near the target protein HSD17B4. Our finding that ART1 induces ferroptotic cell death by targeting HSD17B4 provides a promising mechanism to develop new therapeutics for cancer treatment.

Supporting Information

Supporting Information is available and includes Figures S1–S5 and experimental details on the synthesis of artemisinin derivatives.

DOI: 10.31635/ccschem.021.202000691
Corrected Citation: *CCS Chem.* **2022**, 4, 304–317
Previous Citation: *CCS Chem.* **2021**, 3, 664–677
Link to VoR: https://doi.org/10.31635/ccschem.021.202000691

Conflict of Interest

The authors declare no competing financial interests.

Funding Information

This work was supported by the National Natural Science Foundation of China (no. 21532002 to Z.-J.Y. and J.Z.; no. 21761142001 to Z.-J.Y.).

Acknowledgments

The authors thank Prof. Y. Wu at SIOC and Prof. K. A. Woerpel at NYU for providing unnatural organic peroxides, K2 Oncology Co., Ltd. for the PDTO samples, Y. Zou and Y. Xiao for mass spectrometry support, and Z. Xie and Z. Zhu for the help in mass spectrometry analysis of lipids. The authors also thank V. Kagan and H. Bayir for helpful discussion.

References

1. Degterev, A.; Hitomi, J.; Germscheid, M.; Ch'en, I. L.; Korkina, O.; Teng, X.; Abbott, D.; Cuny, G. D.; Yuan, C.; Wagner, G. J. Identification of RIP1 Kinase as a Specific Cellular Target of Necrostatins. *Nat. Chem. Biol.* **2008**, *4*, 313–321.
2. Khosravi-Far, R.; White, E. *Programmed Cell Death in Cancer Progression and Therapy*; Springer Science & Business Media: New York, **2007**; Vol. 615.
3. Lockshin, R. A.; Zakeri, Z. Programmed Cell Death and Apoptosis: Origins of the Theory. *Nat. Rev. Mol. Cell Biol.* **2001**, *2*, 545–550.
4. Dixon, S. J.; Lemberg, K. M.; Lamprecht, M. R.; Skouta, R.; Zaitsev, E. M.; Gleason, C. E.; Patel, D. N.; Bauer, A. J.; Cantley, A. M.; Yang, W. S. Ferroptosis: An Iron-Dependent Form of Nonapoptotic Cell Death. *Cell* **2012**, *149*, 1060–1072.
5. Yang, W. S.; SriRamaratnam, R.; Welsch, M. E.; Shimada, K.; Skouta, R.; Viswanathan, V. S.; Cheah, J. H.; Clemons, P. A.; Shamji, A. F.; Clish, C. B. Regulation of Ferroptotic Cancer Cell Death by GPX4. *Cell* **2014**, *156*, 317–331.
6. Yang, W. S.; Kim, K. J.; Gaschler, M. M.; Patel, M.; Shchepinov, M. S.; Stockwell, B. R. Peroxidation of Polyunsaturated Fatty Acids by Lipoxygenases Drives Ferroptosis. *Proc. Natl. Acad. Sci. U. S. A.* **2016**, *113*, E4966–E4975.
7. Doll, S.; Proneth, B.; Tyurina, Y. Y.; Panzilius, E.; Kobayashi, S.; Ingold, I.; Irmler, M.; Beckers, J.; Aichler, M.; Walch, A. ACSL4 Dictates Ferroptosis Sensitivity by Shaping Cellular Lipid Composition. *Nat. Chem. Biol.* **2017**, *13*, 91–98.
8. Gaschler, M. M.; Andia, A. A.; Liu, H.; Csuka, J. M.; Hurlocker, B.; Vaiana, C. A.; Heindel, D. W.; Zuckerman, D. S.; Bos, P. H.; Reznik, E. FINO 2 Initiates Ferroptosis through GPX4 Inactivation and Iron Oxidation. *Nat. Chem. Biol.* **2018**, *14*, 507–515.
9. Kagan, V. E.; Mao, G.; Qu, F.; Angeli, J. P. F.; Doll, S.; St Croix, C.; Dar, H. H.; Liu, B.; Tyurin, V. A.; Ritov, V. B. Oxidized Arachidonic and Adrenic PEs Navigate Cells to Ferroptosis. *Nat. Chem. Biol.* **2017**, *13*, 81–90.
10. Shimada, K.; Skouta, R.; Kaplan, A.; Yang, W. S.; Hayano, M.; Dixon, S. J.; Brown, L. M.; Valenzuela, C. A.; Wolpaw, A. J.; Stockwell, B. R. Global Survey of Cell Death Mechanisms Reveals Metabolic Regulation of Ferroptosis. *Nat. Chem. Biol.* **2016**, *12*, 497–503.
11. Wang, J.; Zhang, J.; Shi, Y.; Xu, C.; Zhang, C.; Wong, Y. K.; Lee, Y. M.; Krishna, S.; He, Y.; Lim, T. K. Mechanistic Investigation of the Specific Anticancer Property of Artemisinin and Its Combination with Aminolevulinic Acid for Enhanced Anticolorectal Cancer Activity. *ACS Cent. Sci.* **2017**, *3*, 743–750.
12. Hangauer, M. J.; Viswanathan, V. S.; Ryan, M. J.; Bole, D.; Eaton, J. K.; Matov, A.; Galeas, J.; Dhruv, H. D.; Berens, M. E.; Schreiber, S. L. Drug-Tolerant Persister Cancer Cells Are Vulnerable to GPX4 Inhibition. *Nature* **2017**, *551*, 247–250.
13. Viswanathan, V. S.; Ryan, M. J.; Dhruv, H. D.; Gill, S.; Eichhoff, O. M.; Seashore-Ludlow, B.; Kaffenberger, S. D.; Eaton, J. K.; Shimada, K.; Aguirre, A. J. Dependency of a Therapy-Resistant State of Cancer Cells on a Lipid Peroxidase Pathway. *Nature* **2017**, *547*, 453–457.
14. Chen, G. Q.; Benthani, F. A.; Wu, J.; Liang, D.; Bian, Z. X.; Jiang, X. Artemisinin Compounds Sensitize Cancer Cells to Ferroptosis by Regulating Iron Homeostasis. *Cell Death Differ.* **2020**, *27*, 242–254.
15. Jiang, Y.; Zhao, X.; Huang, J.; Li, J.; Upputuri, P. K.; Sun, H.; Han, X.; Pramanik, M.; Miao, Y.; Duan, H.; Pu, K.; Zhang, R. Transformable Hybrid Semiconducting Polymer Nanozyme for Second Near-Infrared Photothermal Ferrotherapy. *Nat. Commun.* **2020**, *11*, 1–13.
16. He, S.; Jiang, Y.; Li, J.; Pu, K. Semiconducting Polycomplex Nanoparticles for Photothermal Ferrotherapy of Cancer. *Angew. Chem. Int. Ed.* **2020**, *132*, 10720–10725.
17. Tu, Y. Artemisinin—A Gift from Traditional Chinese Medicine to the World (Nobel Lecture). *Angew. Chem. Int. Ed.* **2016**, *55*, 10210–10226.
18. Eastman, R. T.; Fidock, D. A. Artemisinin-Based Combination Therapies: A Vital Tool in Efforts to Eliminate Malaria. *Nat. Rev. Microbiol.* **2009**, *7*, 864–874.
19. Asawamahasakda, W.; Ittarat, I.; Pu, Y.-M.; Ziffer, H.; Meshnick, S. R. Reaction of Antimalarial Endoperoxides with Specific Parasite Proteins. *Antimicrob. Agents Chemother.* **1994**, *38*, 1854–1858.
20. Meshnick, S. R. The Mode of Action of Antimalarial Endoperoxides. *Trans. R. Soc. Trop. Med. Hyg.* **1994**, *88*, 31–32.
21. Berdelle, N.; Nikolova, T.; Quiros, S.; Efferth, T.; Kaina, B. Artesunate Induces Oxidative DNA Damage, Sustained DNA Double-Strand Breaks, and the ATM/ATR Damage Response in Cancer Cells. *Mol. Cancer Ther.* **2011**, *10*, 2224–2233.
22. Drenberg, C. D.; Buaboonnam, J.; Orwick, S. J.; Hu, S.; Li, L.; Fan, Y.; Shelat, A. A.; Guy, R. K.; Rubnitz, J.; Baker, S. D. Evaluation of Artemisinins for the Treatment of Acute Myeloid Leukemia. *Cancer Chemother. Pharmacol.* **2016**, *77*, 1231–1243.

DOI: 10.31635/ccschem.021.202000691
Corrected Citation: *CCS Chem.* **2022**, 4, 304–317
Previous Citation: *CCS Chem.* **2021**, 3, 664–677
Link to VoR: https://doi.org/10.31635/ccschem.021.202000691

23. Lu, M.; Sun, L.; Zhou, J.; Yang, J. Dihydroartemisinin Induces Apoptosis in Colorectal Cancer Cells through the Mitochondria-Dependent Pathway. *Tumor Biol.* **2014**, *35*, 5307–5314.
24. Tin, A. S.; Sundar, S. N.; Tran, K. Q.; Park, A. H.; Poindexter, K. M.; Firestone, G. L. Antiproliferative Effects of Artemisinin on Human Breast Cancer Cells Requires the Downregulated Expression of the E2F1 Transcription Factor and Loss of E2F1-Target Cell Cycle Genes. *Anticancer Drugs* **2012**, *23*, 370–379.
25. Zhang, C. Z.; Pan, Y.; Cao, Y.; Lai, P. B.; Liu, L.; Chen, G. G.; Yun, J. Histone Deacetylase Inhibitors Facilitate Dihydroartemisinin-Induced Apoptosis in Liver Cancer in Vitro and in Vivo. *Plos One* **2012**, *7*, e39870.
26. Chen, T.; Li, M.; Zhang, R.; Wang, H. Dihydroartemisinin Induces Apoptosis and Sensitizes Human Ovarian Cancer Cells to Carboplatin Therapy. *J. Cell Mol. Med.* **2009**, *13*, 1358–1370.
27. Firestone, G. L.; Sundar, S. N. Anticancer Activities of Artemisinin and Its Bioactive Derivatives. *Exp. Rev. Mol. Med.* **2009**, *11*, e32.
28. Wang, Z.; Hu, W.; Zhang, J.-L.; Wu, X.-H.; Zhou, H.-J. Dihydroartemisinin Induces Autophagy and Inhibits the Growth of Iron-Loaded Human Myeloid Leukemia K562 Cells via ROS Toxicity. *FEBS Open Bio.* **2012**, *2*, 103–112.
29. Wong, Y. K.; Xu, C.; Kalesh, K. A.; He, Y.; Lin, Q.; Wong, W. F.; Shen, H. M.; Wang, J. Artemisinin as an Anticancer Drug: Recent Advances in Target Profiling and Mechanisms of Action. *Med. Res. Rev.* **2017**, *37*, 1492–1517.
30. Zhang, Z. S.; Wang, J.; Shen, Y. B.; Guo, C. C.; Sai, K.; Chen, F. R.; Mei, X.; Han, F.; Chen, Z. P. Dihydroartemisinin Increases Temozolomide Efficacy in Glioma Cells by Inducing Autophagy. *Oncol. Lett.* **2015**, *10*, 379–383.
31. Eichhorn, T.; Schloissnig, S.; Hahn, B.; Wendler, A.; Mertens, R.; Lehmann, W.; Krauth-Siegel, R.; Efferth, T. Bioinformatic and Experimental Fishing for Artemisinin-Interacting Proteins from Human Nasopharyngeal Cancer Cells. *Mol. Biosyst.* **2012**, *8*, 1311–1318.
32. Fujita, T.; Felix, K.; Pinkaew, D.; Hutadilok-Towatana, N.; Liu, Z.; Fujise, K. Human Fortilin Is a Molecular Target of Dihydroartemisinin. *FEBS Lett.* **2008**, *582*, 1055–1060.
33. Ravindra, K. C.; Ho, W. E.; Cheng, C.; Godoy, L. C.; Wishnok, J. S.; Ong, C. N.; Wong, W. F.; Wogan, G. N.; Tannenbaum, S. R. Untargeted Proteomics and Systems-Based Mechanistic Investigation of Artesunate in Human Bronchial Epithelial Cells. *Chem. Res. Toxicol.* **2015**, *28*, 1903–1913.
34. Zhou, Y.; Li, W.; Xiao, Y. Profiling of Multiple Targets of Artemisinin Activated by Hemin in Cancer Cell Proteome. *ACS Chem. Biol.* **2016**, *11*, 882–888.
35. Möller, G.; Leenders, F.; van Grunsven, E. G.; Dolez, V.; Qualmann, B.; Kessels, M. M.; Markus, M.; Krazeisen, A.; Husen, B.; Wanders, R. Characterization of the HSD17B4 Gene: D-Specific Multifunctional Protein 2/17β-Hydroxysteroid Dehydrogenase IV. *J. Steroid Biochem. Mol. Biol.* **1999**, *69*, 441–446.
36. Frasinyuk, M. S.; Zhang, W.; Wyrebek, P.; Yu, T.; Xu, X.; Sviripa, V. M.; Bondarenko, S. P.; Xie, Y.; Ngo, H. X.; Morris, A. Developing Antineoplastic Agents that Target Peroxisomal Enzymes: Cytisine-Linked Isoflavonoids as Inhibitors of Hydroxysteroid 17-Beta-Dehydrogenase-4 (HSD17B4). *Org. Biomol. Chem.* **2017**, *15*, 7623–7629.
37. Wanders, R. J.; Waterham, H. R. Biochemistry of Mammalian Peroxisomes Revisited. *Annu. Rev. Biochem.* **2006**, *75*, 295–332.
38. Haapalainen, A. M.; Van Aalten, D. M.; Meriläinen, G.; Jalonen, J. E.; Pirilä, P.; Wierenga, R. K.; Hiltunen, J. K.; Glumoff, T. J. Crystal Structure of the Liganded SCP-2-Like Domain of Human Peroxisomal Multifunctional Enzyme Type 2 at 1.75 Å Resolution. *J. Mol. Biol.* **2001**, *313*, 1127–1138.
39. Haapalainen, A. M.; Koski, M. K.; Qin, Y.-M.; Hiltunen, J. K.; Glumoff, T. Binary Structure of the Two-Domain (3R)-Hydroxyacyl-CoA Dehydrogenase from Rat Peroxisomal Multifunctional Enzyme Type 2 at 2.38 Å Resolution. *Structure* **2003**, *11*, 87–97.
40. Koski, M. K.; Haapalainen, A. M.; Hiltunen, J. K.; Glumoff, T. Crystal Structure of 2-Enoyl-CoA Hydratase 2 from Human Peroxisomal Multifunctional Enzyme Type 2. *J. Mol. Biol.* **2005**, *345*, 1157–1169.
41. Esterbauer, H.; Cheeseman, K. H. Determination of Aldehydic Lipid Peroxidation Products: Malonaldehyde and 4-Hydroxynonenal. *Methods Enzymol.* **1990**, *186*, 407–421.
42. Du, J.; Wang, T.; Li, Y.; Zhou, Y.; Wang, X.; Yu, X.; Ren, X.; An, Y.; Wu, Y.; Sun, W. DHA Inhibits Proliferation and Induces Ferroptosis of Leukemia Cells through Autophagy Dependent Degradation of Ferritin. *Free Radic. Biol. Med.* **2019**, *131*, 356–369.
43. Chen, H.-J.; Wu, Y. Expeditious Entry to the Chamigrane Endoperoxide Family of Natural Products. *Org. Lett.* **2015**, *17*, 592–595.
44. Xu, Z. J.; Wittlin, S.; Wu, Y. Probing the Peroxycarbenium [3+2] Cycloaddition Reactions with 1,2-Disubstituted Ethylenes: Results and Insights. *Chem. Eur. J.* **2017**, *23*, 2031–2034.
45. Zilka, O.; Shah, R.; Li, B.; Friedmann Angeli, J. P.; Griesser, M.; Conrad, M.; Pratt, D. A. On the Mechanism of Cytoprotection by Ferrostatin-1 and Liproxstatin-1 and the Role of Lipid Peroxidation in Ferroptotic Cell Death. *ACS Cent. Sci.* **2017**, *3*, 232.
46. Dixon, S. J.; Winter, G. E.; Musavi, L. S.; Lee, E. D.; Snijder, B.; Rebsamen, M.; Superti-Furga, G.; Stockwell, B. R. Human Haploid Cell Genetics Reveals Roles for Lipid Metabolism Genes in Nonapoptotic Cell Death. *ACS Chem. Biol.* **2015**, *10*, 1604–1609.
47. Kang, S. W.; Lee, S.; Lee, E. K. ROS and Energy Metabolism in Cancer Cells: Alliance for Fast Growth. *Arch. Pharm. Res.* **2015**, *38*, 338–345.
48. Barrera, G. Oxidative Stress and Lipid Peroxidation Products in Cancer Progression and Therapy. *ISRN Oncol.* **2012**, *2012*, 137289.
49. Wang, J.; Zhang, C.-J.; Chia, W. N.; Loh, C. C.; Li, Z.; Lee, Y. M.; He, Y.; Yuan, L.-X.; Lim, T. K.; Liu, M. Haem-Activated Promiscuous Targeting of Artemisinin in *Plasmodium falciparum*. *Nat. Commun.* **2015**, *6*, 1–11.

DOI: 10.31635/ccschem.021.202000691
Corrected Citation: *CCS Chem.* **2022**, 4, 304–317
Previous Citation: *CCS Chem.* **2021**, 3, 664–677
Link to VoR: https://doi.org/10.31635/ccschem.021.202000691